Applied Mathematics & Information Sciences
An International Journal

http://dx.doi.org/10.18576/amis/110613

Unsteady MHD Non-Darcian Flow of a Casson Nanofluid Between Two Parallel Plates with Heat and Mass Transfer

Nabil T. M. El-dabe[1], *H. A. Attia* [2], *M. A. I. Essawy* [3,*], *A. A. Ramadan* [4] *and A. H. Abdel-Hamid*[4]

[1] Department of Mathematics, Faculty of Education, Ain Shams University, Roxy, Cairo, 11757, Egypt.
[2] Department of Engineering Mathematics and Physics, Faculty of Engineering, Fayoum University, El-Fayoum-63415, Egypt.
[3] Higher Technological Institute (HTI), 3^{rd} zone, 7^{th} section-P.O Box NO. 4-6^{th} of October City, Giza, Egypt.
[4] Mathematics Department, Faculty of Science, Beni-Suef University, Beni-Suef - 62511, Egypt.

Received: 23 Dec. 2015, Revised: 10 Oct. 2016, Accepted: 13 Oct. 2016
Published online: 1 Nov. 2017

Abstract: The unsteady MHD Hartmann flow of an incompressible Casson nanofluid bounded by two stationery parallel horizontal plates in a porous medium is studied with heat and mass transfer. A non-Darcy model that obeys the Forchheimer extension is assumed for the characteristics of the porous medium. A uniform and constant pressure gradient is applied in the axial direction whereas a uniform suction and injection are applied in the direction normal to the plates. The two plates are kept at constant and different temperatures and the viscous and porous dissipations are not ignored in the energy equation. Moreover, the concentration of the nanoparticles at the lower plate level differs from that at the upper one, while, both are kept constants. The system of momentum, heat and concentration equations is solved numerically using the finite difference scheme under the appropriate initial and boundary conditions. The effects of the Hall current, the porosity of the medium, inertial damping force, the uniform (suction/ injection) velocity, the non-Newtonian Casson parameter, Hartmann number, Eckert number, Prandtl number, Lewis number, Brownian motion parameter and thermophoretic parameter on the fluid velocity, temperature and nanoparticles concentration distributions are investigated.

Keywords: Non-Darcian flow; Nanofluids; Hall current; Casson fluid; parallel plates; Forchheimer equation; Finite Difference; Numerical solution.

Nomenclature

x, y	Coordinates in horizontal and vertical directions respectively
T_1, T_2	The temperature of lower and upper plates respectively
C_1, C_2	The nanoparticles concentration at the lower and upper plates respectively
dp/dx	The pressure gradient of the fluid
μ	The coefficient of viscosity
ρ	The density of the fluid
K	The Darcy permeability of porous medium
β	The porosity parameter
λ	The inertial coefficient
S	The suction parameter
γ	The dimensionless non-Darcian parameter
c	Specific heat capacity of the fluid
k	Thermal conductivity of the fluid
m	The non-Newtonian Casson parameter
r	The Hall parameter
$\vec{J}$	The current density
B	The Hall factor
B_0	The uniform magnetic field in the positive y-direction
σ	The electric conductivity of the fluid
Ha	Hartmann number

* Corresponding author e-mail: Mohamed.essawy@hti.edu.eg

T	The fluid temperature
u	The velocity component in the x-direction
t	The time
v_0	The constant velocity component in the y-direction
α	The thermal diffusivity
Ec	Eckert number
Pr	Prandtl number
C	The nanoprticles concentration
D_t	The thermophoretic diffusion coefficient
D_b	The Brownian motion coefficient
Nb	The Brownian motion parameter
Nt	The thermophoretic parameter
Le	The Lewis number

1 Introduction

The flow of a viscous fluid between two horizontal parallel plates has important applications as in magnetohydrodynamic (MHD) power generators, MHD pumps, accelerators, aerodynamics heating, electrostatic precipitation, polymer technology, petroleum industry, purification of molten metals from non-metallic inclusions and fluid droplets-sprays [1]. The flow between parallel plates of a Newtonian and non-Newtonian fluid with heat transfer has been examined by many researchers in the hydrodynamic case [2,3] considering constant physical properties. The extension of the problem to the MHD case has attracted the attention of many authors [4, 5,6,7,8].

Previous studies indicate that not much work has been presented yet regarding Casson fluid. This model [9,10, 11] in fact is a plastic fluid that exhibits shear thinning characteristics and that quantifies yield stress and high shear viscosity. Casson fluid model is reduced to a Newtonian fluid at very high wall shear stresses, when wall stress is much greater than yield stress. This fluid has good approximations for many substances such as biological materials, foams, molten chocolate, cosmetics, nail polish, some particulate suspensions, etc. The boundary layer behavior of viscoelastic fluid has technical applications in engineering such as glass fiber, paper production, manufacture of foods, the aerodynamic extrusion of plastic sheets, the polymer extrusion in a melt spinning process and many others [12].

Fluid flow in a porous medium is now one of the most important topics due to its wide applications in both science and engineering [13,14]. In most of the previous work, the Darcy model was adopted when studying porous flows. The Darcy law is sufficient in studying small rate flows where the Reynolds number is very small. For larger Reynolds numbers the Darcy law is insufficient and a variety of models have been implemented in studying flows in porous media. The Darcy-Forchheimer (DF) model is probably the most popular modification to Darcian flow utilized in simulating inertial effects [15,16]. It has been used extensively in chemical engineering analysis and also in materials processing simulations. On the other hand, we may indicate the existence of non-Darcian flow (of different kind) for very low velocity in low-permeability media, [17,18].

Nanofluids are attracting a great deal of interest with their enormous potential to provide enhanced performance properties, particularly with respect to heat transfer. Nanofluids are a new class of fluids that can significantly improve the thermal properties of fluids used as thermal vectors. The term ”nanofluid” refers to a liquid suspension containing tiny particles having diameter less than 100 nm. To extend the fluid applicability, the utilization of nanofluids as superior solid-liquid phase change materials (PCM) for thermal energy storage has been proposed recently. The extension of potential utility of nanofluids requires thermal conductivity measurements and modeling for nanofluids with base liquids other than water and ethylene glycol. However, one of the main applications of nanofluids as heat transfer fluids is in heat exchangers, where the other thermal resistances and increased viscosity will attenuate the nanofluid advantages. The use of additives is a technique applied to enhance the heat transfer performance of base fluids. The thermal conductivity of the ordinary heat transfer fluids is not adequate to meet today’s cooling rate requirements. Nanofluids have been shown to increase the thermal conductivity and convective heat transfer performance of the base liquids. One of the possible mechanisms for the anomalous increase in the thermal conductivity of nanofluids is the Brownian motions of the nanoparticles inside the base fluids. The addition of small particles causes scattering of the incident radiation allowing higher levels of absorption within the fluid. Choi [19] experimentally verified that the addition of small amount of nanoparticles appreciably enhances the effective thermal conductivity of the base fluid. These particles are made up of the metals such as (Al, Cu), oxides (AlO_3), carbides (SiC), nitrides (AlN, SiN) or nonmetals (graphite, carbon nanotubes).

Buongiorno [20] proposed a mathematical model that considers two significant effects namely the Brownian motion and thermophoretic diffusion of nanoparticles.

The characteristic feature of nanofluids is thermal conductivity enhancement, a phenomenon observed by Masuda et al., [21]. This phenomenon suggests the possibility of using nanofluids in advanced nuclear systems [22]. A comprehensive survey of convective transport in nanofluids has been made by Buongiorno [23], who says that a satisfactory explanation for the abnormal increase of the thermal conductivity and viscosity is yet to be found. He focuses on the further heat transfer enhancement observed in the convective situations. Very recently, Kuznetsov and Nield [24] have examined the influence of nanoparticles on the natural convection boundary layer flow past a vertical plate by using a model in which Brownian motion and thermophoresis are accounted for. They have assumed that both the temperature and the nanoparticle fraction are constant along the wall. Further, Nield and Kuznetsov [25] have studied the problem proposed by Cheng and Minkowycz [26] about the natural convection past a vertical plate in a porous medium saturated by a nanofluid. The model used for the nanofluid incorporates the effects of the Brownian motion and thermophoresis.

Attia et al, [27] studied the unsteady non-Darcian flow between two stationery parallel plates in porous medium with heat transfer considering the effect of suction where the fluid motion is subjected to a constant pressure gradient. This problem was studied considering the case of a Couette flow [28]. An extension of this work was presented when the fluid is acted upon by an exponential decaying pressure gradient applied in the axial direction [29,30].

In this paper, the unsteady MHD Hartmann non Darcian flow with heat and mass transfer through a porous medium of an incompressible Casson nanofluid between two infinite horizontal stationery parallel plates is investigated and the DF model is used for the characteristics of the porous medium. A constant pressure gradient is applied in the axial direction and a uniform suction from above and injection from below is imposed in the direction normal to the plates. The two plates are maintained at two different but constant temperatures. Also, the concentration of the nanoparticles at the lower plate differs from that at the upper one, while, both are kept constants. The non-Darcy flow in the porous medium deals with the analysis in which the partial differential equations governing the fluid motion are based on the non-Darcy law (Darcy -Forchheimer flow model) that accounts for the drag exerted by the porous medium [31, 32,33] in addition to the inertial effect [16,34,35,36] The viscous dissipation is taken into consideration in the energy equation. This configuration is a good approximation of some practical situations such as heat exchangers, flow meters, and pipes that connect system components. The cooling of these devices can be achieved by utilizing a porous surface through which a coolant, either a liquid or gas, is forced. Therefore, the results obtained here are important for the design of the wall and the cooling arrangements of these devices.

The governing momentum, energy and concentration equations are solved numerically using the finite difference approximations. The inclusion of the porosity effect, inertial damping force, the velocity of suction, the Hall parameter, the non-Newtonian Casson parameter, Brownian motion parameter and thermophoretic parameter in addition to Hartmann, Eckert, Prandtl and Lewis numbers, leads to some interesting effects, on the velocity, temperature and nanoparticles concentration distributions.

2 Description of the Problem

The two parallel insulating horizontal plates are located at the y = ± h planes and extend from x = - ∞ to ∞ and z = - ∞ to ∞ embedded in a DF porous medium where a high Reynolds number is assumed [15,16]. The lower and upper plates are kept at the two constant temperatures T_1 and T_2, respectively, where $T_2 > T_1$ and a heat source is included, moreover, the concentration of the nanoparticles at the lower plate is set to a constant value C_1 differs from that at the upper one C_2, as shown in Fig. (1). The fluid flows between the two plates in a porous medium where the non-Darcy law (Darcy-Forchheimer flow model) is assumed [16,34,35,36] The motion is driven by a constant pressure gradient dp/dx in the x-direction, and a uniform suction from above and injection from below which are applied at $t = 0$ with velocity v_o in the positive y-direction. A uniform magnetic field B_o is applied in the positive y-direction and is assumed undisturbed as the induced magnetic field is neglected by assuming a very small magnetic Reynolds number. The Hall Effect is taken into consideration and consequently a z-component for the velocity is expected to arise. Due to the infinite dimensions in the x and z-directions all quantities apart from the pressure gradient dp/dx which is assumed constant, are independent of the x and z-coordinates, thus the velocity vector of the fluid is given by:

$$\vec{v}\,(y,t) = u(y,t)\,\vec{i} + v_o\,\vec{j} + w(y,t)\,\vec{k}$$

with the initial and boundary conditions $u = 0$ at $t \leq 0$, and $u = 0$ at $y = \pm h$ for $t > 0$. The temperature $T(y,t)$ at

any point in the fluid satisfies both the initial and boundary conditions $T = T_1$ at $t \leq 0$, $T = T_2$ at $y = +h$, and $T = T_1$ at $y = -h$ for $t > 0$. The nanoparticles concentration $C(y,t)$ at any point in the fluid satisfies both the initial and boundary conditions $C = C_1$ at $t \leq 0$, $C = C_2$ at $y = +h$, and $C = C_1$ at $y = -h$ for $t > 0$.

We also, assume the rheological equation of Casson fluid, reported in [37, 38]

$$\tau_{ij} = \begin{cases} 2\left(\mu_B + \frac{P_y}{\sqrt{2\pi}}\right) e_{ij} & , \quad \pi > \pi_c \\ 2\left(\mu_B + \frac{P_y}{\sqrt{2\pi_c}}\right) e_{ij} & , \quad \pi < \pi_c \end{cases}$$

where, μ_B is the plastic dynamic viscosity of the non-Newtonian fluid, π denotes the product of the component of deformation rate with itself, $\pi = e_{ij}\, e_{ij}$ and e_{ij} is the $(i, j)^{\text{th}}$ component of deformation rate, π_c shows a critical value of this product based on the non-Newtonian model, and P_y is the yield stress of the fluid.

The fluid flow is governed by the momentum equation,

$$\rho \frac{D\vec{v}}{Dt} = \nabla . (\mu \nabla \vec{v}) - \vec{\nabla} P + \vec{J} \wedge \vec{B}_o + \vec{F}_{DF} \qquad (1)$$

If the Hall term is retained, the current density $\vec{J}$ is given by

$$\vec{J} = \sigma(\vec{v} \wedge \vec{B}_o - B(\vec{J} \wedge \vec{B}_o)) \qquad (2)$$

where σ is the electric conductivity of the fluid, and B is the Hall factor. Equation (2) may be solved in $\vec{J}$ to yield:

$$\vec{J} \wedge \vec{B}_o = -\frac{\sigma B_o^2}{1+r^2}\left((u + rw)\,\vec{i} + (w - ru)\,\vec{k}\right) \qquad (3)$$

where $r = \sigma B B_o$, is the Hall parameter. Thus, in terms of Eq. (3), the two components of Eq. (1) read:

$$\begin{aligned} \frac{\partial u}{\partial t} + v_o \frac{\partial u}{\partial y} = & -\frac{1}{\rho_F}\frac{dP}{dx} + \frac{\mu}{\rho_F}\left(1 + \frac{1}{m}\right)\frac{\partial^2 u}{\partial y^2} \\ & - \frac{\sigma B_o^2}{\rho(1+r^2)}(u + rw) - \frac{\mu}{K\rho_F} u - \frac{\lambda}{K} u^2 \end{aligned} \qquad (4)$$

$$\begin{aligned} & \frac{\partial w}{\partial t} + v_o \frac{\partial w}{\partial y} = \\ & \frac{\mu}{\rho_F}\left(1 + \frac{1}{m}\right)\frac{\partial^2 w}{\partial y^2} - \frac{\sigma B_o^2}{\rho(1+r^2)}(w - ru) - \frac{\mu}{K\rho_F} w - \frac{\lambda}{K} w^2 \end{aligned} \qquad (5)$$

Where ρ_F and μ are, respectively, the density of the fluid and the coefficient of viscosity, K is the Darcy permeability of porous medium [31-33], $m = \mu_B \sqrt{2\pi_c}\,/\,p_y$ is the non-Newtonian Casson parameter [12] and λ is the inertial coefficient (i.e. the non-Darcian Forchheimer geometrical constant which is related to the geometry of the porous medium [16]).

The third term in the right side of equations (4) and (5) both represent the electromagnetic force due to the effect of the Hall current. The last two terms in the right side of equations (4) and (5) represent the non-Darcy porosity forces.

To find the temperature distribution inside the fluid we use the energy equation,

$$\begin{aligned} & \frac{\partial T}{\partial t} + v_o \frac{\partial T}{\partial y} = \alpha \frac{\partial^2 T}{\partial y^2} + RD_b\left(\frac{\partial C}{\partial y}\frac{\partial T}{\partial y}\right) \\ & + \frac{RD_t}{T_1}\left(\frac{\partial T}{\partial y}\right)^2 + \frac{\mu}{(\rho c)_F}\left(1 + \frac{1}{m}\right)\left[\left(\frac{\partial u}{\partial y}\right)^2 + \left(\frac{\partial w}{\partial y}\right)^2\right] \\ & + \frac{\mu}{K(\rho c)_F}(u^2 + w^2) + \frac{\sigma B_o^2}{(\rho c)_F(1+r^2)}(u^2 + w^2) \end{aligned} \qquad (6)$$

where, C represents the nanoparticles concentration, while, c and k are, respectively, the specific heat capacity and the thermal conductivity of the fluid. $R = (\rho c)_p$ / $(\rho c)_F$ is the dimensionless parameter that gives the ratio of effective heat capacity of the nanoparticle material to heat capacity of the fluid. Thus value of R will be, therefore, different for different fluids and nanoparticle materials. D_t is the thermophoretic diffusion coefficient and D_b is the Brownian motion coefficient. The last three terms on the right side of Eq. (6) represent the viscous and Joule dissipations effects; the first term is the classical expression of the viscous dissipation for a clear fluid ($K \to \infty$), while, the second term is the viscous dissipation in the Darcy limit ($K \to 0$) [39], for a full discussion for modeling this form of viscous dissipation, see [40,41]. The last term represent the Joule dissipation, we notice that each of these terms has two components; this is because the Hall Effect brings about a velocity w in the z-direction.

To study the nanoparticles concentrations during the fluid motion, we use the concentration equation which is given by [42,43]

$$\frac{\partial C}{\partial t} + v_o \frac{\partial C}{\partial y} = D_b \frac{\partial^2 C}{\partial y^2} + \frac{D_t}{T_1}\frac{\partial^2 T}{\partial y^2} \qquad (7)$$

The density ρ_{nF}, the viscosity μ_{nF}, and the thermal conductivity k_{nF} of the nanofluid are defined, respectively, as [44,45]:

$$\rho_{nF} = (1 - \zeta)\,\rho_F + \zeta\,\rho_p \;, \quad \mu_{nF} = \frac{\mu_F}{(1-\zeta)^{2.5}} \;, \quad \alpha_{nF} = \frac{k_{nF}}{(\rho c_p)_{nF}}$$

where ζ is the solid volume fraction, μ_F is the dynamic viscosity of the base fluid, ρ_F and ρ_p are the densities of the base fluid and the nanoparticle, respectively, the suffixes F, p, and nF denote base fluid, nanoparticle, and nanofluid conditions, respectively, and $(\rho c_p)_{nF}$ is the heat

capacitance of the nanofluid, which are defined as:

$$(\rho c_p)_{nF} = (1-\zeta)(\rho c_p)_F + \zeta(\rho c_p)_p \ ,$$
$$\frac{k_{nF}}{k_F} = \frac{k_p + 2k_F - 2\zeta(k_F - k_p)}{k_p + 2k_F + 2\zeta(k_F - k_p)}$$

where, k_F and k_p are the thermal conductivities of the base fluid and nanoparticle, respectively.

Introducing the following non-dimensional quantities and parameters:

$(\hat{x},\hat{y},\hat{z}) = \frac{(x,y,z)}{h}, \hat{u} = \frac{\rho h u}{\mu}, \hat{w} = \frac{\rho h w}{\mu}, \hat{P} = \frac{P\rho h^2}{\mu^2}, \hat{t} = \frac{t\mu}{\rho h^2}$,
$\hat{T} = \frac{T-T_1}{T_2-T_1}, \hat{C} = \frac{C-C_1}{C_2-C_1}, S = \rho v_o h/\mu, \beta = h^2/K, \gamma = \lambda h/K$,
$Ha^2 = \sigma B_o^2 h^2/\mu, Ec = \mu^2/\rho^2 c h^2 (T_2 - T_1), Pr = \mu c/k$,
$Le = k/\rho c D_b,\ N_b = RD_b(C_2 - C_1)/\alpha$,
$N_t = RD_t(T_2 - T_1)/\alpha T_1$

Equations (4), (5), (6) and (7) are written as (the "hats" will be dropped for convenience):

$$\frac{\partial u}{\partial t} + S\frac{\partial u}{\partial y} = -\frac{dP}{dx} + \left(1+\frac{1}{m}\right)\frac{\partial^2 u}{\partial y^2} - \frac{Ha^2}{(1+r^2)}(u+rw) - \beta u - \gamma u^2 \quad (8)$$

$$\frac{\partial w}{\partial t} + S\frac{\partial w}{\partial y} = \left(1+\frac{1}{m}\right)\frac{\partial^2 w}{\partial y^2} - \frac{Ha^2}{(1+r^2)}(w-ru) - \beta w - \gamma w^2 \quad (9)$$

$$\frac{\partial T}{\partial t} + S\frac{\partial T}{\partial y} = \frac{1}{\Pr}\frac{\partial^2 T}{\partial y^2} + \frac{N_b}{\Pr}\left(\frac{\partial C}{\partial y}\frac{\partial T}{\partial y}\right) + \frac{N_t}{\Pr}\left(\frac{\partial T}{\partial y}\right)^2 + Ec\left(1+\frac{1}{m}\right)\left[\left(\frac{\partial u}{\partial y}\right)^2 + \left(\frac{\partial w}{\partial y}\right)^2\right] + \beta Ec(u^2+w^2) + \frac{Ha^2 Ec}{(1+r^2)}(u^2+w^2) \quad (10)$$

$$\frac{\partial C}{\partial t} + S\frac{\partial C}{\partial y} = \frac{1}{\Pr Le}\frac{\partial^2 C}{\partial y^2} + \frac{1}{\Pr Le}\frac{N_t}{N_b}\frac{\partial^2 T}{\partial y^2} \quad (11)$$

The initial and boundary conditions for the velocity components, temperature and nanoparticles concentration are given respectively by (12), (13) and (14):

$$u = w = 0,\ t \le 0\ \&\ u = w = 0,\ y = \pm 1,\ t > 0 \quad (12)$$

$$t \le 0 : T = 0 \,\&\, t > 0 : T = 1, y = +1 \,\&\, t > 0 : T = 0, y = -1 \quad (13)$$

$$t \le 0 : C = 0 \,\&\, t > 0 : C = 1, y = +1 \,\&\, t > 0 : C = 0, y = -1 \quad (14)$$

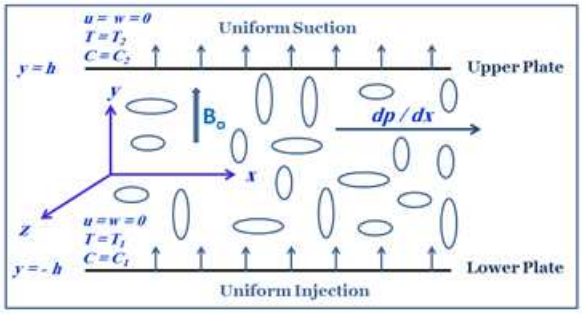

Fig. 1: The geometry of the problem

3 Numerical Solution of the Governing Equations

Equations (8), (9), (10) and (11) are solved numerically using finite differences [46] under the initial and boundary conditions (12), (13) and (14) to determine the velocity, temperature and nanoparticles concentration distributions for different values of the governing parameters β, γ, S, r, m, N_t and N_b with various values of the Hartmann, Prandtl, Eckert and Lewis numbers. The Crank-Nicolson implicit method [47] is applied.

We define the variables $V = \partial u/\partial y$, $M = \partial w/\partial y$, $H = \partial T/\partial y$ and $F = \partial C/\partial y$ to reduce the second order differential equations (8), (9), (10) and (11) to first order differential equations as follows:

$$\frac{\partial u}{\partial t} + SV = -\frac{dP}{dx} + \left(1+\frac{1}{m}\right)\frac{\partial V}{\partial y} - \frac{Ha^2}{(1+r^2)}(u+rw) - \beta u - \gamma u^2 \quad (15)$$

$$\frac{\partial w}{\partial t} + SM = \left(1+\frac{1}{m}\right)\frac{\partial M}{\partial y} - \frac{Ha^2}{(1+r^2)}(w-ru) - \beta w - \gamma w^2 \quad (16)$$

$$\frac{\partial T}{\partial t} + SH = \frac{1}{\Pr}\frac{\partial H}{\partial y} + \frac{N_b}{\Pr}HF + \frac{N_t}{\Pr}H^2 + Ec\left(1+\frac{1}{m}\right)(V^2+M^2) + \beta Ec(u^2+w^2) + \frac{Ha^2 Ec}{(1+r^2)}(u^2+w^2) \quad (17)$$

$$\frac{\partial C}{\partial t} + SF = \frac{1}{\Pr Le}\frac{\partial F}{\partial y} + \frac{1}{\Pr Le}\frac{N_t}{N_b}\frac{\partial H}{\partial y} \quad (18)$$

3.1 Finite Difference Representations

The computational domain is divided into meshes each of dimension Δt and Δy in the time and space respectively

as shown in figure (2). Finite difference equations relating the variables are obtained by writing the equations at the midpoint of the computational cell and then replacing the different terms by their second order central difference approximation in y direction. The diffusion terms are replaced by the average of the central differences at two successive time-levels. Finally, the resulting block tri-diagonal system is solved using the generalized Thomas-algorithm [48].

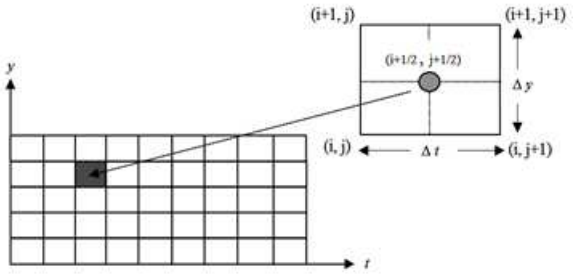

Fig. 2: Finite differences mesh layout

The finite difference representations for the resulting first order differential equations (15), (16), (17) and (18) take the form

$$\frac{u_{i+1,j+1}-u_{i+1,j}+u_{i,j+1}-u_{i,j}}{2\Delta t}+S\frac{V_{i+1,j+1}+V_{i+1,j}+V_{i,j+1}+V_{i,j}}{4}$$
$$=-\frac{dp}{dx}+\left(1+\frac{1}{m}\right)\frac{V_{i+1,j+1}+V_{i+1,j}-V_{i,j+1}-V_{i,j}}{2\Delta y}-\frac{Ha^2}{4(1+r^2)}$$
$$\left[\left(u_{i+1,j+1}+u_{i+1,j}+u_{i,j+1}+u_{i,j}\right)+r\left(w_{i+1,j+1}+w_{i+1,j}\right.\right.$$
$$\left.\left.+w_{i,j+1}+w_{i,j}\right)\right]-\beta\frac{u_{i+1,j+1}+u_{i+1,j}+u_{i,j+1}+u_{i,j}}{4},$$
$$-\gamma\frac{\left(u_{i+1,j+1}+u_{i+1,j}+u_{i,j+1}+u_{i,j}\right)\left(u_{i+1,j}+u_{i,j}\right)}{8} \tag{19}$$

$$\frac{w_{i+1,j+1}-w_{i+1,j}+w_{i,j+1}-w_{i,j}}{2\Delta t}+S\frac{M_{i+1,j+1}+M_{i+1,j}+M_{i,j+1}+M_{i,j}}{4}$$
$$=\left(1+\frac{1}{m}\right)\frac{M_{i+1,j+1}+M_{i+1,j}-M_{i,j+1}-M_{i,j}}{2\Delta y}-\frac{Ha^2}{4(1+r^2)}$$
$$\left[\left(w_{i+1,j+1}+w_{i+1,j}+w_{i,j+1}+w_{i,j}\right)-r\left(u_{i+1,j+1}\right.\right.$$
$$\left.\left.+u_{i+1,j}+u_{i,j+1}+u_{i,j}\right)\right]-\beta\frac{w_{i+1,j+1}+w_{i+1,j}+w_{i,j+1}+w_{i,j}}{4}$$
$$-\gamma\frac{\left(w_{i+1,j+1}+w_{i+1,j}+w_{i,j+1}+w_{i,j}\right)\left(w_{i+1,j}+w_{i,j}\right)}{8} \tag{20}$$

$$\frac{\left(T_{i+1,j+1}-T_{i+1,j}+T_{i,j+1}-T_{i,j}\right)}{2\Delta t}+S\frac{\left(H_{i+1,j+1}+H_{i+1,j}+H_{i,j+1}+H_{i,j}\right)}{4}$$
$$=\frac{1}{\Pr}\frac{\left(H_{i+1,j+1}+H_{i+1,j}-H_{i,j+1}-H_{i,j}\right)}{2\Delta y}$$
$$+\frac{N_t}{\Pr}\frac{\left(H_{i+1,j+1}+H_{i+1,j}+H_{i,j+1}+H_{i,j}\right)\left(H_{i+1,j}+H_{i,j}\right)}{8}+\frac{N_b}{\Pr}$$
$$\frac{\left(H_{i+1,j+1}+H_{i,j+1}\right)\left(F_{i+1,j}+F_{i,j}\right)+\left(F_{i+1,j+1}+F_{i,j+1}\right)\left(H_{i+1,j}+H_{i,j}\right)}{4}$$
$$+Ec\left(1+\frac{1}{m}\right)\left[\frac{\left(V_{i+1,j+1}+V_{i+1,j}+V_{i,j+1}+V_{i,j}\right)\left(V_{i+1,j}+V_{i,j}\right)}{8}\right.$$
$$\left.+\frac{\left(M_{i+1,j+1}+M_{i+1,j}+M_{i,j+1}+M_{i,j}\right)\left(M_{i+1,j}+M_{i,j}\right)}{8}\right]$$
$$+Ec\left(\beta+\frac{Ha^2}{(1+r^2)}\right)\left[\frac{\left(u_{i+1,j+1}+u_{i+1,j}+u_{i,j+1}+u_{i,j}\right)\left(u_{i+1,j}+u_{i,j}\right)}{8}\right.$$
$$\left.+\frac{\left(w_{i+1,j+1}+w_{i+1,j}+w_{i,j+1}+w_{i,j}\right)\left(w_{i+1,j}+w_{i,j}\right)}{8}\right] \tag{21}$$

$$\frac{\left(C_{i+1,j+1}-C_{i+1,j}+C_{i,j+1}-C_{i,j}\right)}{2\Delta t}+S\frac{\left(F_{i+1,j+1}+F_{i+1,j}+F_{i,j+1}+F_{i,j}\right)}{4}=$$
$$\frac{1}{\Pr Le}\frac{\left(F_{i+1,j+1}+F_{i+1,j}-F_{i,j+1}-F_{i,j}\right)}{2\Delta y}$$
$$+\frac{1}{\Pr Le}\frac{N_t}{N_b}\frac{\left(H_{i+1,j+1}+H_{i+1,j}-H_{i,j+1}-H_{i,j}\right)}{2\Delta y} \tag{22}$$

3.2 Generalized Thomas Algorithm

The linearized systems of difference equations represent banded matrices that can be solved by different methods. These systems have block-diagonal matrices which have very well defined structures. One of the very powerful methods to solve this system is the Thomas algorithm, because we need not to store the matrix coefficients, which reduces the computational time. The momentum, energy and concentration equations are rewritten respectively in the following forms

$$a_1u_l+a_2u_k+a_3V_l+a_4V_k+a_5w_l+a_6w_k+a_7M_l+a_8M_k=a_9 \tag{23}$$

$$b_1w_l+b_2w_k+b_3M_l+b_4M_k+b_5u_l+b_6u_k+b_7V_l+b_8V_k=b_9 \tag{24}$$

$$p_1T_l+p_2T_k+p_3H_l+p_4H_k+p_5C_l+p_6C_k+p_7F_l+p_8F_k=p_9 \tag{25}$$

$$q_1C_l+q_2C_k+q_3F_l+q_4F_k+q_5T_l+q_6T_k+q_7H_l+q_8H_k=q_9 \tag{26}$$

where, a_n, b_n,p_n and q_n with (n = 1, 2, …, 9) are the coefficients of the difference equations (23-26) that parallel to equations (19-22) respectively, l and k are counters to (i, j+1) and (i+1, j+1), respectively (for simplicity).

Firstly, the momentum equations (19, 20) are solved to compute the velocity components u, w and their derivatives V and M respectively. We may write the generalized Thomas-algorithm as in the following steps [46]. The unknowns are written as

$$u_l=\bar{u}_lV_l+\tilde{u}_lM_l+\hat{u}_l \tag{27}$$

$$w_l=\bar{w}_lV_l+\tilde{w}_lM_l+\hat{w}_l \tag{28}$$

$$V_l = \bar{V}_k V_k + \tilde{V}_k M_k + \hat{V}_k \quad (29)$$

$$M_l = \bar{M}_k V_k + \tilde{M}_k M_k + \hat{M}_k \quad (30)$$

where, the variables $\bar{u}_l$, $\tilde{u}_l$, $\hat{u}_l$, $\bar{w}_l$, $\tilde{w}_l$, $\hat{w}_l$, $\bar{V}_k$, $\tilde{V}_k$, $\hat{V}_k$, $\bar{M}_k$, $\tilde{M}_k$, $\hat{M}_k$ represent the Thomas coefficients. The equations are relating u and w to their derivatives V and M, respectively. From the definitions of V and M we obtain:

$$\frac{u_k - u_l}{\Delta y} = \frac{V_l + V_k}{2} \quad , \quad \frac{w_k - w_l}{\Delta y} = \frac{M_l + M_k}{2}$$

Or,

$$u_k = (\bar{u}_l + \Delta y/2) V_l + (\Delta y/2) V_k + \tilde{u}_l M_l + \hat{u}_l \quad (31)$$

and

$$w_k = (\tilde{w}_l + \Delta y/2) M_l + (\Delta y/2) M_k + \bar{w}_l V_l + \hat{w}_l \quad (32)$$

Or,

$$u_k = \bar{u}_k V_k + \tilde{u}_k M_k + \hat{u}_k \quad (33)$$

and

$$w_k = \bar{w}_k V_k + \tilde{w}_k M_k + \hat{w}_k \quad (34)$$

After many operations in the equations (23), (24) and (27-34), we may compute the required coefficients from the following relations:

$$\bar{u}_k = (\Delta y/2) + (\bar{u}_l + \Delta y/2) \bar{V}_k + \tilde{u}_l \bar{M}_k \quad (35)$$

$$\tilde{u}_k = (\bar{u}_l + \Delta y/2) \tilde{V}_k + \tilde{u}_l \tilde{M}_k \quad (36)$$

$$\hat{u}_k = (\bar{u}_l + \Delta y/2) \hat{V}_k + \tilde{u}_l \hat{M}_k + \hat{u}_l \quad (37)$$

$$\bar{w}_k = (\Delta y/2) + (\bar{w}_l + \Delta y/2) \bar{V}_k + \tilde{w}_l \bar{M}_k \quad (38)$$

$$\tilde{w}_k = (\bar{w}_l + \Delta y/2) \tilde{V}_k + \tilde{w}_l \tilde{M}_k \quad (39)$$

$$\hat{w}_k = (\bar{w}_l + \Delta y/2) \hat{V}_k + \tilde{w}_l \hat{M}_k + \hat{w}_l \quad (40)$$

$$\bar{V}_k = (g_3 h_2 - g_2 h_3)/(g_1 h_2 - g_2 h_1) \quad (41)$$

$$\tilde{V}_k = (g_4 h_2 - g_2 h_4)/(g_1 h_2 - g_2 h_1) \quad (42)$$

$$\hat{V}_k = (g_5 h_2 - g_2 h_5)/(g_1 h_2 - g_2 h_1) \quad (43)$$

$$\bar{M}_k = (g_1 h_3 - g_3 h_1)/(g_1 h_2 - g_2 h_1) \quad (44)$$

$$\tilde{M}_k = (g_1 h_4 - g_4 h_1)/(g_1 h_2 - g_2 h_1) \quad (45)$$

$$\hat{M}_k = (g_1 h_5 - g_5 h_1)/(g_1 h_2 - g_2 h_1) \quad (46)$$

Where,

$$g_1 = a_1 \bar{u}_l + a_2 (\bar{u}_l + \Delta y/2) + a_3 + a_5 \bar{w}_l + a_6 \bar{w}_l \quad (47)$$

$$g_2 = a_1 \tilde{u}_l + a_2 \tilde{u}_l + a_5 \tilde{w}_l + a_6 (\tilde{w}_l + \Delta y/2) + a_7 \quad (48)$$

$$g_3 = -[(\Delta y/2) a_2 + a_4] \quad (49)$$

$$g_4 = -[(\Delta y/2) a_6 + a_8] \quad (50)$$

$$g_5 = a_9 - a_1 \hat{u}_l - a_2 \hat{u}_l - a_5 \hat{w}_l - a_6 \hat{w}_l \quad (51)$$

$$h_1 = b_1 \bar{w}_l + b_2 \bar{w}_l + b_5 \bar{u}_l + b_6 (\bar{u}_l + \Delta y/2) + b_7 \quad (52)$$

$$h_2 = b_1 \tilde{w}_l + b_2 (\tilde{w}_l + \Delta y/2) + b_3 + b_5 \tilde{u}_l + b_6 \tilde{u}_l \quad (53)$$

$$h_3 = -[(\Delta y/2) b_6 + b_8] \quad (54)$$

$$h_4 = -[(\Delta y/2) b_2 + b_4] \quad (55)$$

$$h_5 = b_9 - b_1 \tilde{w}_l - b_2 \hat{w}_l - b_5 \hat{u}_l - b_6 \hat{u}_l \quad (56)$$

Secondly, the energy and concentration equations (21, 22) are solved to compute the temperature T and the concentration C and their derivatives H and F respectively. We may write the generalized Thomas-algorithm as in the following steps [46]. The unknowns are written as

$$T_l = \bar{T}_l H_l + \tilde{T}_l F_l + \hat{T}_l \quad (57)$$

$$C_l = \bar{C}_l H_l + \tilde{C}_l F_l + \hat{C}_l \quad (58)$$

$$H_l = \bar{H}_k H_k + \tilde{H}_k F_k + \hat{H}_k \quad (59)$$

$$F_l = \bar{F}_k H_k + \tilde{F}_k F_k + \hat{F}_k \quad (60)$$

Where, the variables $\bar{T}_l$, $\tilde{T}_l$, $\hat{T}_l$, $\bar{C}_l$, $\tilde{C}_l$, $\hat{C}_l$, $\bar{H}_k$, $\tilde{H}_k$, $\hat{H}_k$, $\bar{F}_k$, $\tilde{F}_k$, $\hat{F}_k$ represent the Thomas coefficients. The equations are

relating T and C to their derivatives H and F, respectively. From the definitions of H and F we obtain:

$$\frac{T_k - T_l}{\Delta y} = \frac{H_l + H_k}{2} \ , \quad \frac{C_k - C_l}{\Delta y} = \frac{F_l + F_k}{2}$$

Or,

$$T_k = (\bar{T}_l + \Delta y/2)\, H_l + (\Delta y/2) H_k + \tilde{T}_l\, F_l + \hat{T}_l \quad (61)$$

and

$$C_k = (\tilde{C}_l + \Delta y/2)\, F_l + (\Delta y/2) F_k + \bar{C}_l\, H_l + \hat{C}_l \quad (62)$$

Or,

$$T_k = \bar{T}_k H_k + \tilde{T}_k\, F_k + \hat{T}_k \quad (63)$$

and

$$C_k = \bar{C}_k H_k + \tilde{C}_k\, F_k + \hat{C}_k \quad (64)$$

After many operations in the equations (25, 26) and (57-64), we may compute the required coefficients from the following relations:

$$\bar{T}_k = (\Delta y/2) + (\bar{T}_l + \Delta y/2)\, \bar{H}_k + \tilde{T}_l\, \bar{F}_k \quad (65)$$

$$\tilde{T}_k = (\bar{T}_l + \Delta y/2) \tilde{H}_k + \tilde{T}_l\, \tilde{F}_k \quad (66)$$

$$\hat{T}_k = (\bar{T}_l + \Delta y/2) \hat{H}_k + \tilde{T}_l\, \hat{F}_k + \hat{T}_l \quad (67)$$

$$\bar{C}_k = (\Delta y/2) + (\bar{C}_l + \Delta y/2)\, \bar{H}_k + \tilde{C}_l\, \bar{F}_k \quad (68)$$

$$\tilde{C}_k = (\bar{C}_l + \Delta y/2) \tilde{H}_k + \tilde{C}_l\, \tilde{F}_k \quad (69)$$

$$\hat{C}_k = (\bar{C}_l + \Delta y/2) \hat{H}_k + \tilde{C}_l\, \hat{F}_k + \hat{C}_l \quad (70)$$

$$\bar{H}_k = (l_3 f_2 - l_2 f_3)/(l_1 f_2 - l_2 f_1) \quad (71)$$

$$\tilde{H}_k = (l_4 f_2 - l_2 f_4)/(l_1 f_2 - l_2 f_1) \quad (72)$$

$$\hat{H}_k = (l_5 f_2 - l_2 f_5)/(l_1 f_2 - l_2 f_1) \quad (73)$$

$$\bar{F}_k = (l_1 f_3 - l_3 f_1)/(l_1 f_2 - l_2 f_1) \quad (74)$$

$$\tilde{F}_k = (l_1 f_4 - l_4 f_1)/(l_1 f_2 - l_2 f_1) \quad (75)$$

$$\hat{F}_k = (l_1 f_5 - l_5 f_1)/(l_1 f_2 - l_2 f_1) \quad (76)$$

Where,

$$l_1 = p_1 \bar{T}_l + p_2(\bar{T}_l + \Delta y/2) + p_3 + p_5 \bar{C}_l + p_6 \bar{C}_l \quad (77)$$

$$l_2 = p_1 \tilde{T}_l + p_2 \tilde{T}_l + p_5 \tilde{C}_l + p_6(\tilde{C}_l + \Delta y/2) + p_7 \quad (78)$$

$$l_3 = -\left[(\Delta y/2)\, p_2 + p_4\right] \quad (79)$$

$$l_4 = -\left[(\Delta y/2)\, p_6 + p_8\right] \quad (80)$$

$$l_5 = p_9 - p_1\, \hat{T}_l - p_2\, \hat{T}_l - p_5\, \hat{C}_l - p_6\, \hat{C}_l \quad (81)$$

$$f_1 = q_1 \bar{C}_l + q_2\, \bar{C}_l + q_5 \bar{T}_l + q_6\, (\bar{T}_l + \Delta y/2) + q_7 \quad (82)$$

$$f_2 = q_1 \tilde{C}_l + q_2\, (\tilde{C}_l + \Delta y/2) + q_3 + q_5 \tilde{T}_l + q_6 \tilde{T}_l \quad (83)$$

$$f_3 = -\left[(\Delta y/2)\, q_6 + q_8\right] \quad (84)$$

$$f_4 = -\left[(\Delta y/2)\, q_2 + q_4\right] \quad (85)$$

$$f_5 = q_9 - q_1\, \hat{C}_l - q_2\, \hat{C}_l - q_5\, \hat{T}_l - q_6\, \hat{T}_l \quad (86)$$

Computations of the coefficients are started from y = -1 with known velocity, temperature and concentration (u(-1,t) = 0, w(-1,t) = 0, T(-1,t) = 0 and C(-1,t) = 0) from the boundary conditions equations (12-14). Since V, M, H and F are independent on u, w, T and C, respectively, then $\bar{u}_l$, $\tilde{u}_l$, $\hat{u}_l$, $\bar{w}_l$, $\tilde{w}_l$, $\hat{w}_l$, $\bar{T}_l$, $\tilde{T}_l$, $\hat{T}_l$, $\bar{C}_l$, $\tilde{C}_l$, $\hat{C}_l$, take zero values using equations (29), (30), (59) and (60). Thus, all coefficients (up to upper plate) are computed directly from the above equations (35-56) and (65-86). Computations of unknowns u, w, T, C, V, M, H and F are started at the upper plate with known components (u = 0, w = 0, T = 1 and C = 1) using equations (27-86). The above procedure is repeated to modify the unknowns u, w, T, C, V, M, H and F.

All calculations have been carried out for dP/dx = -5, while the results obtained in a covering range for the porosity parameter, $0.0 \leq \beta \leq 2.0$ [27] and the non-Darcian parameter, $0.0 \leq \gamma \leq 2.0$ as [27, 48]. The parameters N_b and N_t can take any value in the interval $(0, \infty)$, that the larger the values of N_b and N_t, the greater will be the strength of the corresponding effects, while, the deviation in the profiles only occur for the values of N_t and N_b in the range (0, 2), [42]. It is found that the unsteady results reduce to those reported in [27,49] for a

clear fluid in the case of Newtonian fluid and Darcian model. These comparisons lend confidence in the accuracy and correctness of the solutions.

4 Results and Discussion

This work describes a system of PDEs governing the motion of a non-Newtonian nanofluid obeys the Casson model with heat and mass transfer. The fluid flow is through a nondarcian porous medium (Darcy-Forchheimer kind) between two infinite parallel permeable plates. The problem is solved numerically with the help of the finite difference method. The formulas of the velocity components, temperature and concentration are obtained as functions of the physical parameters of the problem. The effects of these parameters on these solutions are illustrated numerically and graphically through a set of figures to reinforce the parametric study of the fluid flow.

Figure (3) shows the time progression of the velocity components, temperature and nanoparticles concentration profiles till the steady state with (β = 1, γ = 1, m = 0.5, r = 1, Ha = 1, Pr = 1, Ec = 0.2, N_t = 0.5, N_b = 0.5 and Le = 10). It is observed that the velocity components u and w, the temperature T and the nanoparticles concentration C increase monotonously with time and that u and w reach the steady state faster than T and C, which is expected, since u and w act as the source of temperature. It is clear from fig. (3-I, II) that the velocity charts are asymmetric about the (y = 0) plane because of the suction.

Figure (4) depicts the influence of the suction parameter ($S > 0$) on the velocity, temperature, and nanoparticle volume fraction profiles. Increasing the suction parameter decreases the velocity components as in Fig. (4-I, II). The heated fluid is pushed towards the wall where the buoyancy forces can act to retard the fluid due to the high influence of the Brownian motion, while, this effect acts to decrease the wall shear stress. Figure (4-III) exhibits the decrease in the temperature T with increasing S. On the other hand, the nanoparticle volume fraction C decreases with increasing S at early flow times before it starts to increase with increasing S till reaching its steady state as shown in Fig. (4-IV).

Fig. (5) exhibits the marked effect of the porosity parameter β on the time development of u, w, T and C. It is obvious from fig. (5-I, II) that increasing β decreases u and w and their steady state time as a result of increasing the resistive porosity force on u and w, moreover, increasing β decreases the temperature and its steady state time as shown in Fig.(5-III). Furthermore, the nanoparticle concentration decreases with increasing the porosity parameter at early flow times before it starts to increase with increasing ($\beta > 0$) till reaching its steady state as presented in Fig.(5-IV). It should be mentioned that the highest concentration is obtained in the case of a non porous medium (β = 0).

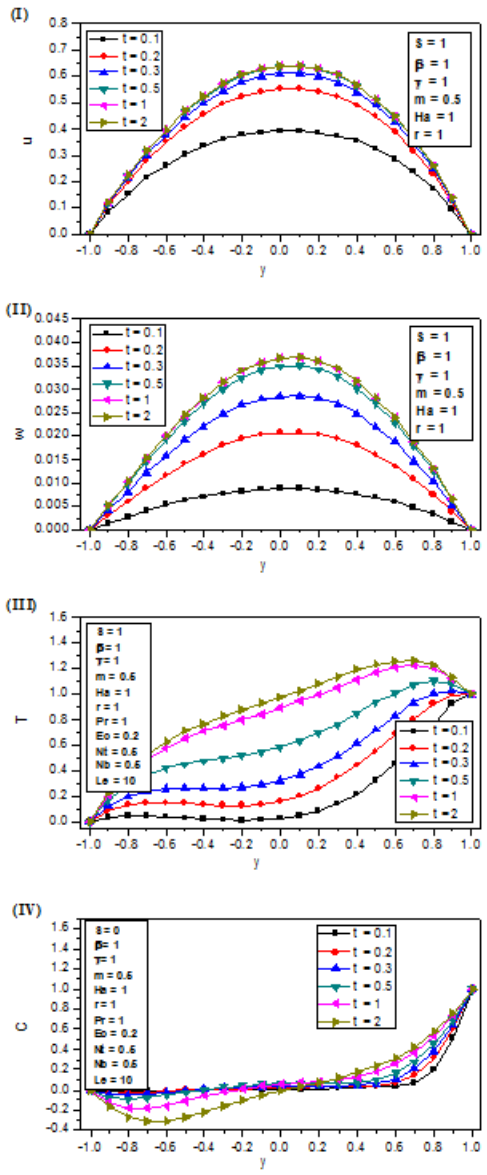

Fig. 3: Time development of (I) the velocity u, (II) the velocity w, (III) the temperature T, and (IV) the nanoparticles concentration C.

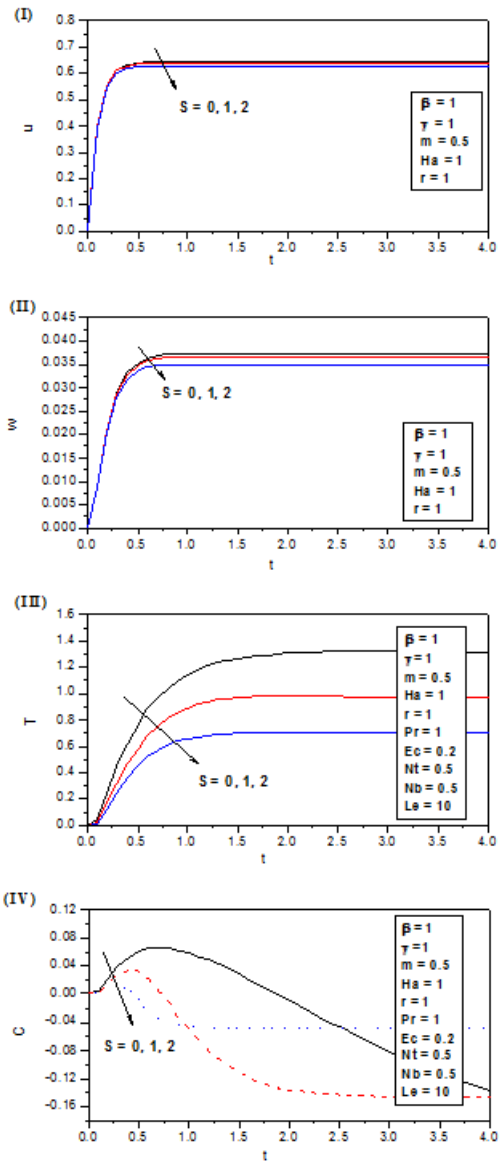

Fig. 4: Effect of the suction parameter S on the time development of (I) the velocity u, (II) the velocity w, (III) the temperature T, and (IV) the nanoparticles concentration C at the center of the channel $(y = 0)$.

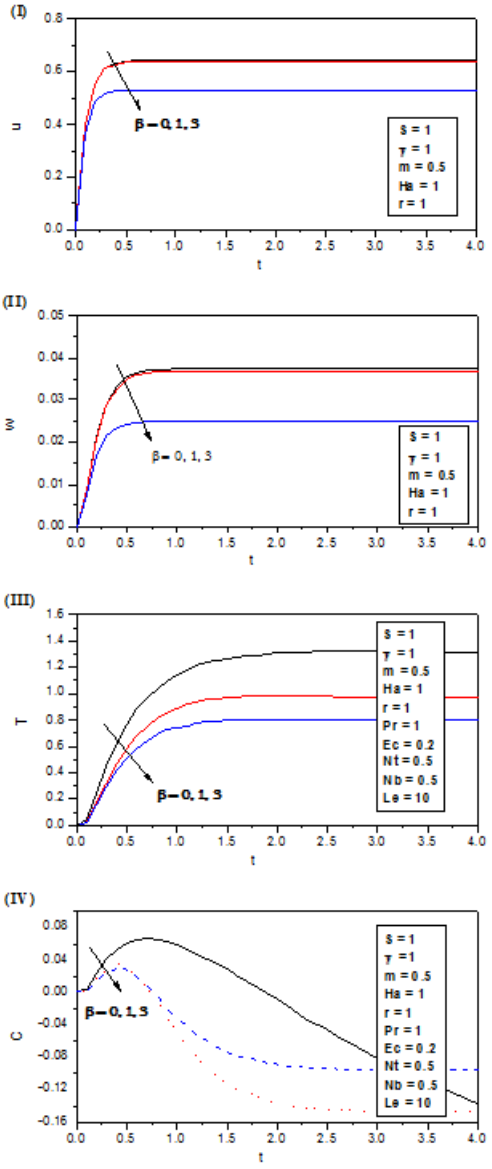

Fig. 5: Effect of the porosity parameter β on the time development of (I) the velocity u, (II) the velocity w, (III) the temperature T, and (IV) the nanoparticles concentration C at the center of the channel (y = 0).

The non-Darcian parameter γ affects the time development of u, w, T and C. Increasing γ decreases the velocities u, w and their steady state times as presented in Fig. (6-I, II) which reflects the expected resistance because of the inertial damping forces.

On the other hand, Fig.(6-III) emphasizes that increasing γ decreases T and its steady state time, as the increase in γ decreases u, w which, in turn, decreases the viscous dissipation which decreases T. The value (γ = 0) in Fig. (6) means that the fluid flows with total absence of the inertial drag and the Darcian case is obtained to provide higher temperature values and an easier quick path for the fluid flow.

In Fig. (6-IV), as the non-Darcy parameter increases, the nanoparticle concentration profile increases, which confirms that increasing γ reduces the intensity of the

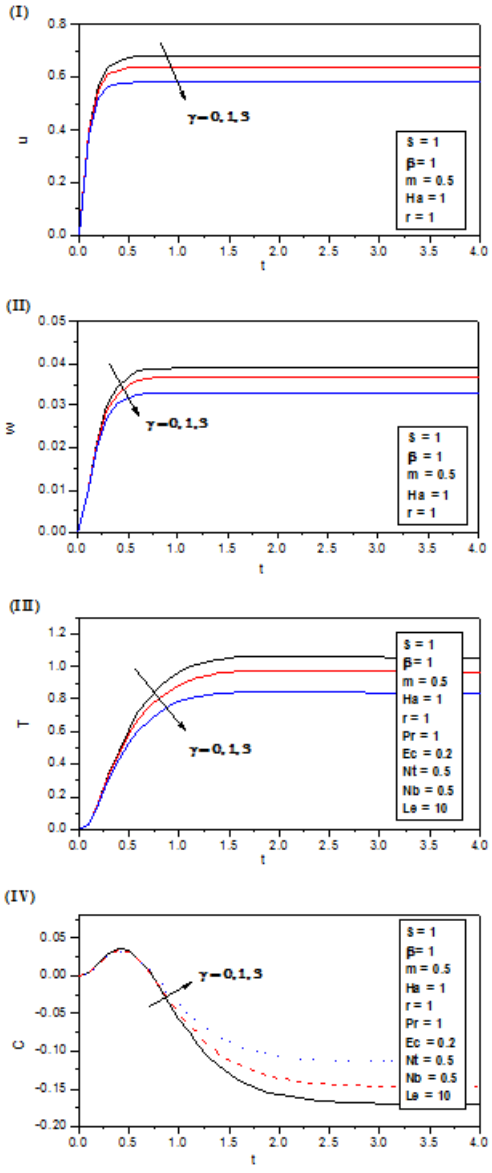

Fig. 6: Effect of the non-darcian parameter γ on the time development of (I) the velocity u, (II) the velocity w, (III) the temperature T, and (IV) the nanoparticles concentration C at the center of the channel (y = 0).

flow but enhances the nanoparticle volume fraction profile. Hence, the non-Darcy parameter has an important role in controlling the flow field.

Fig. (7) shows the effect of the non-Newtonian Casson fluid parameter *m* on the velocity, temperature, and the nanoparticle volume fraction profiles. It is observed that increasing the value of *m* increases the velocity and temperature values, while a reduction in the nanoparticle volume fraction profile is obtained. It should be noted that a large increase in the non-Newtonian Casson fluid parameter *m* indefinitely reduces the problem to the Newtonian fluid case.

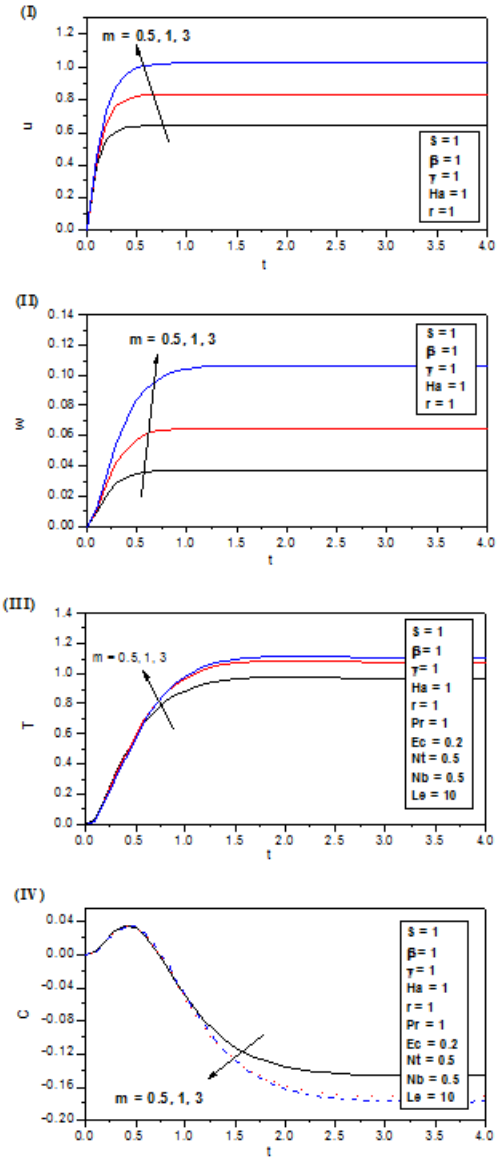

Fig. 7: Effect of the non-Newtonian Casson parameter *m* on the time development of (I) the velocity *u*,(II) the velocity *w*, (III) the temperature *T*, and (IV) the nanoparticles concentration *C* at the center of the channel (y = 0).

Figure (8-I) shows that *u* increases with increasing the Hall parameter *r* as the effective conductivity (= σ/ (1 +

r^2)) decreases with increasing r which reduces the magnetic damping force on u.

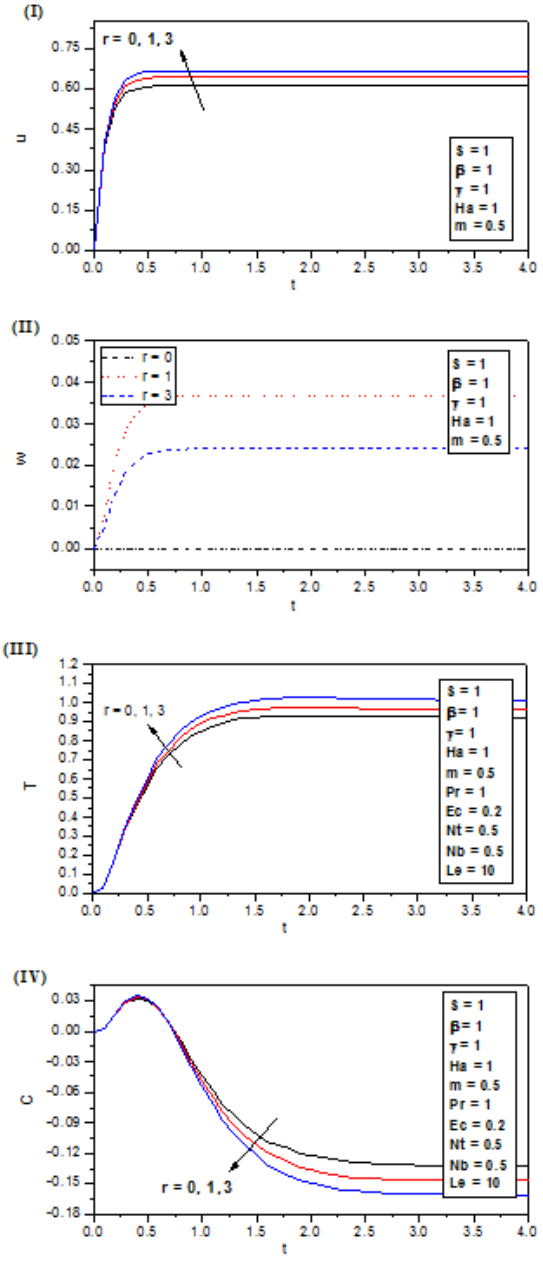

Fig. 8: Effect of the Hall parameter r on the time development of (I) the velocity u,(II) the velocity w, (III) the temperature T, and (IV) the nanoparticles concentration C at the center of the channel (y = 0).

It is observed also that the time at which u reaches its steady state value increases with increasing r.

In Fig. (8-II), the velocity component w increases with increasing the Hall parameter (r = 0 up to 1) which corresponds to an increase in the driving force term $(rHa^2u/(1+r^2))$ in Eq. (9) which pumps the flow in the z-direction. However, increasing the Hall parameter ($r>$ 1) decreases the effective conductivity that results in reducing the driving force and then, decreases w. The temperature T increases with increasing the Hall parameter r due to the increase in the Joule and viscous dissipations as shown in fig (8-III). Moreover, an interesting overshooting is obtained in the concentration profiles that the nanoparticle volume fraction increases at early flow times before it starts to decrease with increasing the Hall parameter r till reaching its steady state as presented in Fig.(8-IV).

Fig (9) shows that the velocity component u and the temperature T decrease while, the velocity component w increases with increasing the Hartman number Ha. Furthermore, Fig.(8-IV) shows that the nanoparticles concentration profiles decrease at early flow times before it starts to increase with increasing the Hartman number Ha till reaching its steady state.

We notice from Fig. (10) that Prandtl number Pr has the same influence on temperature profile as well as on nanoparticle fraction at early flow times, as the increase in Pr has decreasing the behavior for both T and C which may be attributed to the definition of Prandtl number as a ratio of kinematic viscosity to thermal diffusivity. Consequently, for higher values of Prandtl number it reduces the thermal diffusivity. The same behavior can be observed for nanoparticle volume concentration against Prandtl number when we compare temperature profiles with nanoparticles concentration except at the later times of flow where an elevation in the temperature profiles is recognized with increasing Pr. It is worth pointing here that the liquid metals are characterized by small values of ($Pr << 1$), which have high thermal conductivity but low viscosity, while large values of ($Pr >> 1$) correspond to high-viscosity oils. Specifically, Prandtl number Pr = 0.72, 1.0 and 7.0 correspond to air, electrolyte solution such as salt water and water, respectively [50]. In our computations we have chosen Pr = 1 to retrieve all the graphical results.

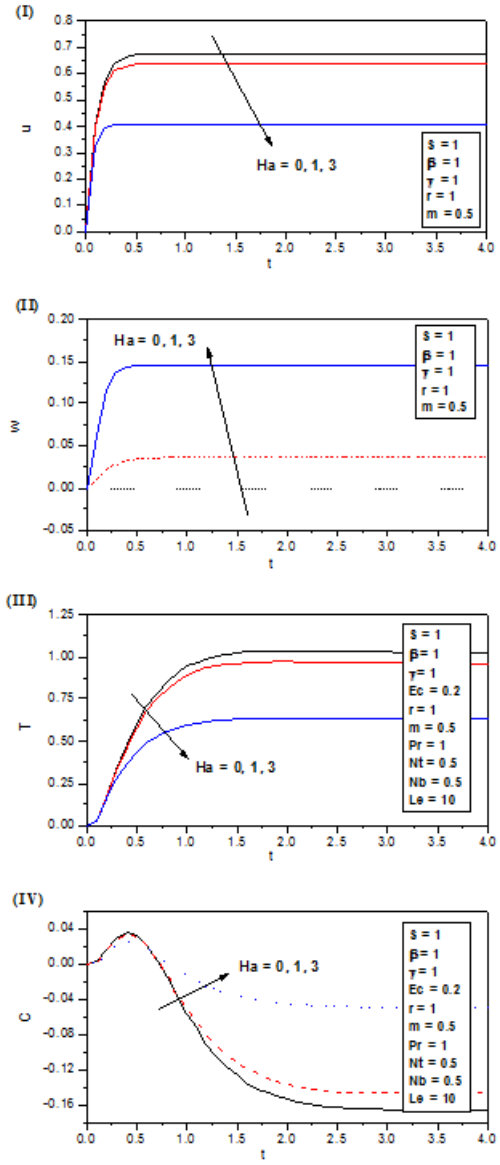

Fig. 9: Effect of the Hartmann number *Ha* on the time development of (I) the velocity *u*, (II) the velocity *w*, (III) the temperature *T*, and (IV) the nanoparticles concentration *C* at the center of the channel (y = 0).

The dimensionless temperature profile is plotted for various values of Eckert number in Fig (11-I). It is obvious that the increase of Eckert number causes an increase of the nanofluid temperature and physically this can be totally verified, because when the friction on the plate increases due to fluid viscosity, more heat is generated and as a result the nanofluid temperature increases. Furthermore, the presence of viscous

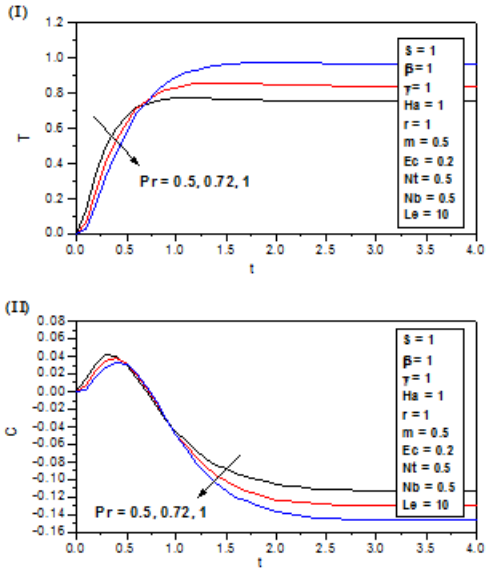

Fig. 10: Effect of the Prandtl number *Pr* on the time development of (I) the temperature *T* and (II) the nanoparticles concentration *C* at the center of the channel (y = 0).

dissipation in the energy equation acts as an internal heat source due to the action of viscous stresses. Fig (11-II) depicts the decreasing effect on the nanoparticles concentration profile with increasing the viscous dissipation exemplified in increasing the Eckert number.

Fig.(12-I) clarifies that the temperature increases with increasing the thermophoretic parameter N_t. Furthermore, the nanoparticle volume fraction increases at early flow times before it starts to decrease with increasing N_t till reaching its steady state as shown in Fig.(12-II). From the physical point of view, an increase in the thermophoretic effect generates a larger mass flux due to temperature gradient which in turn raises the concentration. This mechanism therefore, assists the diffusion of the nanoparticles and elevates the concentration profile with the beginning of the fluid motion while, distinctive peaks occur at earlier flow times for higher values of the thermophoretic parameter N_t.

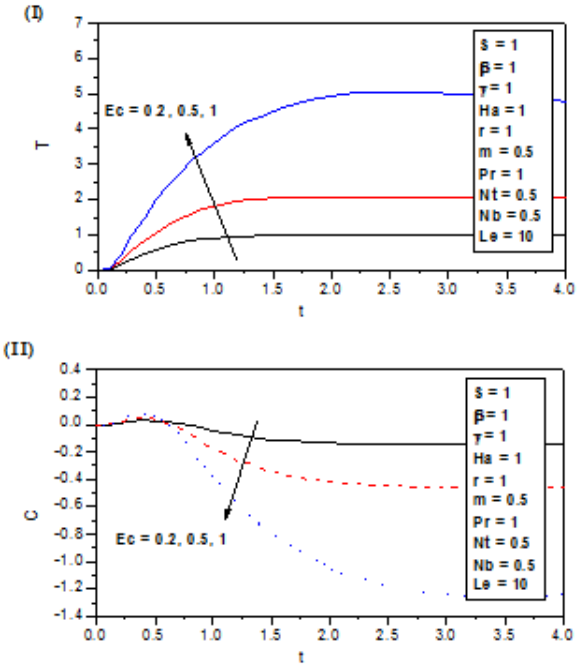

Fig. 11: Effect of the Eckert number Ec on the time development of (I) the temperature T and (II) the nanoparticles concentration C at the center of the channel (y = 0).

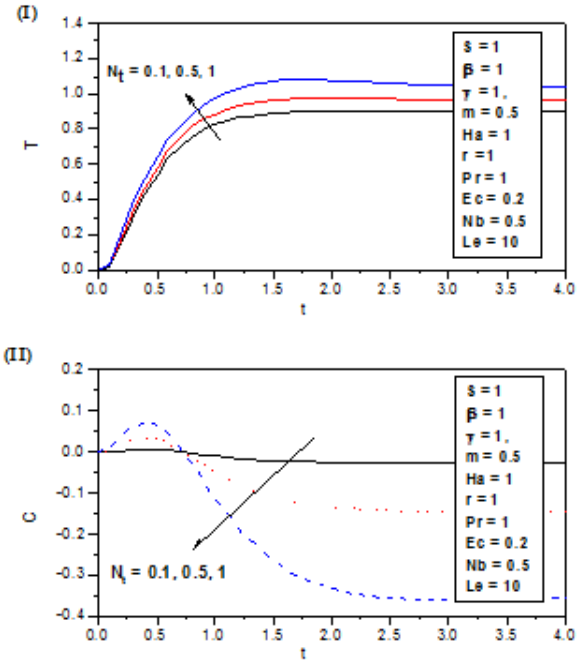

Fig. 12: Effect of the thermophoresis parameter N_t on the time development of (I) the temperature T and (II) the nanoparticles concentration C at the center of the channel (y = 0).

Fig. (13) is prepared to present the effect of the Brownian motion exemplified in the parameter N_b on the temperature distribution and the volume fraction of nanoparticles. The temperature of the fluid decreases with the increase in N_b. On the other hand, the nanoparticle volume fraction decreases at early flow times with increasing N_b and then it starts to increase till reaching its steady state. It is interesting to note that the Brownian motion of nanoparticles at molecular and Nano scale levels, is a key to the Nano scale mechanism governing their thermal behaviors. In nanofluid systems, due to the size of the nanoparticles, the Brownian motion takes place, which can affect the heat transfer properties. As the particle size scale approaches to the nanometer scale, the particle Brownian motion and its effect on the surrounding liquids play an important role in the heat transfer. However, the nanoparticles concentration is negligibly affected for the values of N_b beyond 2.0.

As Lewis number Le defines the ratio of thermal diffusivity to mass (nanoparticle species) diffusivity, it is used to characterize fluid flows where there is simultaneous heat and mass transfer. The temperature increases with increasing the Lewis number as in Fig. (14-I). Furthermore, there is a fall in the nanoparticle concentration with increasing the Lewis number at early flow times, and then an elevation in the concentration profiles is obtained reaching the steady state.

5 Conclusions

The unsteady non-Darcian MHD Hartmann flow through a porous medium between two stationery parallel plates of an incompressible Casson nanofluid was studied with heat and mass transfer in the presence of uniform suction and injection considering different modes of viscous dissipation. The velocity, temperature and nanoparticles concentration are found to increase monotonously with time and that the velocity reaches the steady state faster than the temperature and nanoparticles concentration. The effects of the physical parameters governing the fluid motion are investigated. It is found that increasing the porosity, inertial damping and suction or injection velocity have a marked effect on decreasing the velocity distribution in an inverse proportionality manner, while,

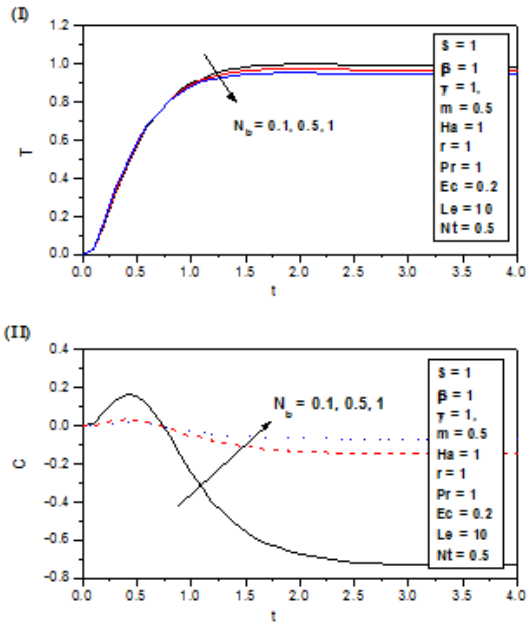

Fig. 13: Effect of the Brownian motion parameter N_b on the time development of (I) the temperature T and (II) the nanoparticles concentration C at the center of the channel (y = 0).

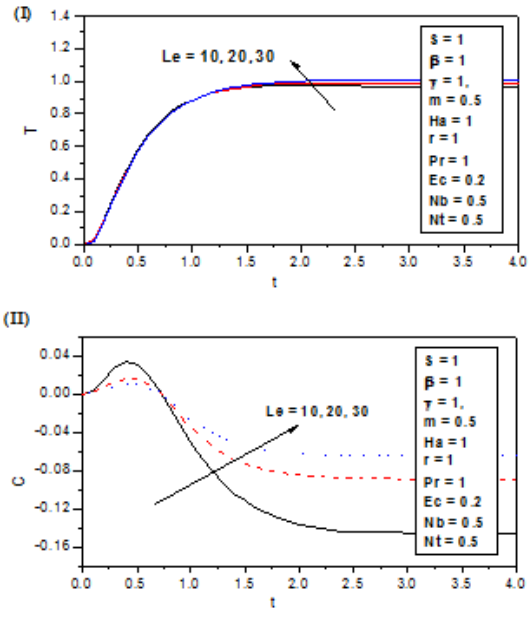

Fig. 14: Effect of the Lewis number Le on the time development of (I) the temperature T and (II) the nanoparticles concentration C at the center of the channel (y = 0).

increasing the non-Newtonian Casson parameter increases the velocity profiles. The increase in the Hall parameter increases the velocity component u and decreases the velocity component w, while, increasing the Hartmann number decreases u but, increases w. Furthermore, increasing β, γ, Ha, S and N_b decreases the temperature; on the other hand, increasing m, Pr, r, Ec, Le and N_t increases the temperature. Studying the nanoparticles concentration behavior results in an obvious decrease in the nanoparticles concentration with increasing m, Pr, r, Ec and N_t, while the nanoparticles volume fraction increses with incresing β, γ, Ha, S, Le and N_b. Various cases were monitored passing through the fluid flow in a non-porous medium, the Darcian flow model and the non-Darcian flow in a porous medium which showed the greatest flow resistance resulting in lower velocity and temperature values but higher concentrations of the nanoparticles.

6 Applications

The future nanofluids research areas include, but are not limited to: emerging synthesis techniques, geothermal power extraction, automotive industry, modification of optical, magnetic, and electronic properties of materials, mass transport, boiling phenomena, waste heat collection, absorption and conversion of radiation, optics, cancer treatment, controlling of fluid motion, consumer goods, electronics, Solar energy harvesting, nuclear power generation, and surfaces and catalysts. The other important area which has seen increasing interest is hyperthermia treatments that requires dispersed nanoparticles to selectively attach to diseased regions. This wide breadth of recent and promised future research has primarily been due to the rapid advances and increasing control in nano-material fabrication techniques.

References

[1] J. Hartmann and F. Lazarus, Kgl. Danske Videnskab. Selskab, Mat.-Fys. Medd., 15, 6, (1937).
[2] A. Orhan, A. Mete, Applied Energy, 83, 856, (2006).
[3] B. Tudor, B. Ioana, Appl Math Comp., 215, 2673, (2009).
[4] R. A. Alpher, Int J Heat and Mass Transfer, 3, 108, (1961).
[5] S. D. Nigam, S. N. Singh, Quart J Mech Appl Math., 13, 85, (1960).
[6] H. A. Attia, African J. Math. Phys., 2, 97, (2005).
[7] H. A. Attia, Kragujevac Journal of Science, 31, 11, (2009).

[8] S. Erik, K. Vajravelu, A. Robert, G. Van, and I. Pop, Comm Non Sc Num Sim., 16, 266, (2011).
[9] N. Casson, In Reheology of Dipersed system. Peragamon press, Oxford, (1959).
[10] M. Nakamura, T. Sawada, J. Biomechanical Eng., 110, 137, (1988).
[11] R. B. Bird, G. C. Dai, B. J. Yarusso, Rev Chem Eng, 1,1, (1983).
[12] V. R. Prasad, A. S. Rao, O. A. Bg, J Appl Computat Math., 2: 127. doi:10.4172/2168-9679.1000127, (2013).
[13] A.E. Scheidegger, The physics of flow through porous media, University of Toronto, (1974).
[14] M. Kaviany, Principles of heat transfer in porous media, Springer, (1995).
[15] N. Jeong, D. H. Choi, C. L. Lin, 16, 2240, (2006).
[16] F. Khani, A. Farmany, M. Ahmad zadeh Raji, Abdul Aziz, F. Samadi, Commun Nonlinear Sci Numer Simulat., 14, 3867, (2009).
[17] Y. Yuedong and GeJiali, Petroleum Science, 8, 55, (2011).
[18] H. H. Liu and J. Birkholzer, Journal of Hydrology, 475, 242, (2012).
[19] S.U.S. Choi, Enhancing thermal conductivity of fluids with nanoparticle, in: D.A. Siginer H.P. Wang (Eds.), Developments and Applications of Non-Newtonian Flows, Vol. FED 231, ASME, New York, pp. 99-105, (1995).
[20] J. Buongiorno, J. Heat Transfer, 128, 240, (2006).
[21] H. Masuda, A. Ebata, K. Teramae, and N. Hishinuma, Netsu Bussei, 7, 227, (1993).
[22] J. Buongiorno and W. Hu, Proceedings of International Congress on Advances in Nuclear Power Plants, Carran Associate, lnc., Seoul, 5705, (2005).
[23] J. Buongiorno, ASME Journal of Heat Transfer, 128, 240, (2006).
[24] A. V. Kuznetsov, D. A. Nield, International Journal of Thermal Sciences, 49, 243, (2010).
[25] D. A. Nield and A. V. Kuznetsov, International Journal of Heat and Mass Transfer, 52 (25-26), 5792, (2009).
[26] P. Cheng and W. J. Minkowycz, Journal of Geophysical Research, 82, 2040, (1977).
[27] H.A. Attia, M.A.I. Essawy, A.H. Khater and A.A. Ramadan, Bulgarian Chemical Communications, 46, 616, (2014).
[28] M.A.I. Essawy and H.A. Attia, International Journal of Mathematical Engineering and Science, 3, 1, (2014).
[29] H.A. Attia, M.A.I. Essawy, A.H. Khater and A.A. Ramadan, International Journal of Basic Sciences & Applied Research, 2, 669, (2013).
[30] H.A. Attia, M.A.I. Essawy, A.H. Khater and A.A. Ramadan, Proceedings of the Eleventh International Conference of Fluid Dynamics (ICFD11), Egypt, (2013).
[31] N. T. El-Dabe , CAN. J. PHYS., 64, 84, (1986).
[32] D.B. Ingham, I. Pop, Transport phenomena in porous media, Pergamon, Oxford, (2002).
[33] N. T. Eldabe, M. Y. Abou-zeid, Arab J Sci Eng., 39, 5045, (2014).
[34] A. K. Singh, P. Agnihotri, N.P. Singh, A. K. Singh, International Journal of Heat and Mass Transfer, 54, 1111, (2011).
[35] N. T. El dabe and S. N. Sallam, Can. J. Phys., 83, 1241, (2005).
[36] D. Pal, H. Mondal, Commun. Nonlinear Sci. Numer. Simulat., 17, 672, (2012).
[37] N. T. M. Eldabe, B. M. Agoor and H. Alame, Journal of Fluids, 2014, 1-12, (2014).
[38] S. Mukhopadhyay, Chin. Phys. B, 22, 1, (2013) .
[39] A.K. Al-Hadhrami, L. Elliott, D.B. Ingham, Transp. Porous Media, 49, 265, (2002).
[40] A. K. Al-Hadhrami, Fluid Flows Through Channels of Composite Materials, Ph D Thesis, University of Leeds, Leeds, (2001).
[41] D. A. Nield, Transport in Porous Media, 41, 349, (2000).
[42] M. M. Hashmi, T. Hayat, A. Alsaedi, Nonlinear Analysis: Modelling and Control, 17, 418, 2012.
[43] K. Das, P. R. Duari, P. K. Kundu, Alexandria Engineering Journal, 53, 737, 2014.
[44] S. M. Aminossadati and B. Ghasemi, European Journal of Mechanics-B/Fluids, 28, 630, (2009).
[45] N. Anbuchezhian, K. Srinivasan, K. Chandrasekaran and R. Kandasamy, Appl. Math. Mech.-Engl. Ed., 33, 765, (2012).
[46] W.F. Ames, Numerical solutions of partial differential equations, 2nd ed., Academic Press, New York, (1977).
[47] A.R. Mitchell, D.F. Griffiths, The Finite Difference Method in Partial Differential Equations , John Wiley, New York, (1980).
[48] M. F. EL-Amin and N. A. Ebrahiem, Transport in Porous Media, 64, 1, (2006).
[49] H.A. Attia, M.A.M. Abdeen, and A.E. Abdin, Journal of Engineering Physics and Thermophysics, 86, 723, (2013).
[50] M.Z. Salleh, R. Nazar, I. Pop, J. Taiwan Inst. Chem. Eng., 41, 651, (2010).

Nabil T. El-Dabe (Ph.D; 1980), He is an Emeritus Professor of Applied Mathematics at Ain-Shams University. He has worked as the chairman of mathematics department, Ain-Shams University, (from 1999-2009). He has more than 150 published research papers in reputed international journals of mathematical sciences. He is a reviewer for many international journals in the specialization of applied mathematics and fluid mechanics. He supervised many M.Sc and Ph.D theses in the field of applied mathematics, mathematical modeling, and fluid mechanics research.

Hazem A. Attia Professor of Engineering Mathematics, chairman of the Department of Engineering Mathematics and Physics (2010 up till now); Fayoum University, Egypt. He has worked as the Dean of Faculty of Engineering, Fayoum University, (from 2011-2015). He has recieved his Ph.D in 1993 from College of Engineering and Mines, The University of Arizona, USA. He is a supervisor of many M.Sc and Ph.D theses in the frame of fluid mechanics, heat transfer, and numerical analysis. He has published more than 310 papers in his specialized field; and is a scientific reviewer for about 95 international journals and conferences. He is an editor of 6 international scientific magazines.

Mohamed A. Essawy lecturer of Applied Mathematics at (HTI), Egypt. He is interesting in Fluid mechanics research; specially; nanofluids, transport in porous media, heat & mass transfer, mathematical modeling and numerical analysis. He has a list of 12 scientific papers. He is a scientific reviewer of 4 international journals and conferences of the field of mathematical and physical sciences. He has attended and participated in several international conferences and workshops. Also, he was invited to visit and participate in the ICTP international activities in Italy, 2015.

Ahmed A. Ramadan is a Professsor of Pure Mathematics and Vice-Dean of faculty of Science at Beni-Suef University, Egypt. He received his Ph.D in pure mathematics. He has about 140 publications in international cited journals of pure and applied mathematical sciences. He is an editor and a scientific reviewer for several international journals.

Alaa H. Abdel-Hamid is an Associate Professor of Mathematical Statistics at Beni-Suef University. His research areas include statistical inference, accelerated life tests, prediction, Bayes inference and mixture of distribution. He has published about 25 scientific papers in the field of applied mathematics and statistics.